ACS OMEGA

Article

Cite This: ACS Omega 2019, 4, 58−64

http://pubs.acs.org/journal/acsodf

Effect of Calcium Ions and Disulfide Bonds on Swelling of Virus Particles

Roi Asor,[†,‡] Daniel Khaykelson,[†,‡] Orly Ben-nun-Shaul,[§] Ariella Oppenheim,[§] and Uri Raviv*[,†,‡]

[†]Institute of Chemistry and [‡]Center for Nanoscience and Nanotechnology, The Hebrew University of Jerusalem, Edmond J. Safra Campus, Givat Ram, Jerusalem 9190401, Israel

[§]Department of Haematology, The Hebrew University-Hadassah Medical School, Ein Karem, Jerusalem 91120, Israel

ABSTRACT: Multivalent ions affect the structure and organization of virus nanoparticles. Wild-type simian virus 40 (wt SV40) is a nonenveloped virus belonging to the polyomavirus family, whose external diameter is 48.4 nm. Calcium ions and disulfide bonds are involved in the stabilization of its capsid and are playing a role in its assembly and disassembly pathways. Using solution small-angle X-ray scattering (SAXS), we found that the volume of wt SV40 swelled by about 17% when both of its calcium ions were chelated by ethylene glycol-bis(2-aminoethylether)-*N*,*N*,*N*′,*N*′-tetraacetic acid and its disulfide bonds were reduced by dithiothreitol. By applying osmotic stress, the swelling could be reversed. DNA-containing virus-like particles behaved in a similar way. The results provide insight into the structural role of calcium ions and disulfide bonds in holding the capsid proteins in compact conformation.

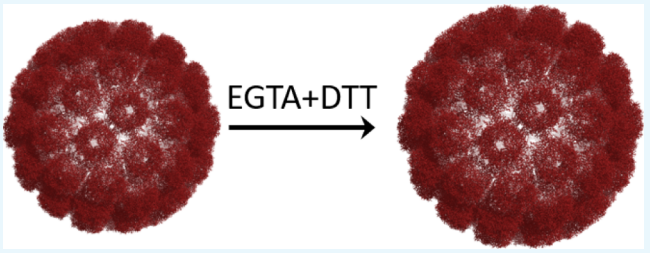

INTRODUCTION

Viruses are evolved examples of self-assembled structures that are functional and sophisticated biological machines. Virus nanoparticles, empty virus-like particles (VLPs), or polymer-containing VLPs (PC-VLPs) may be fabricated into functional materials or nanostructure devices, serve as protein nanocapsules, nanocarriers for metallic nanoparticles, drug or gene delivery, biosensors, or as nanoreactors for catalysis.[1−9] The surfaces of virus nanoparticles present a complex, nonuniform pattern of charged, polar, and hydrophobic residues, which can be tuned by pH.[10]

Wild-type simian virus 40 (wt SV40) is a spherical nonenveloped virus belonging to the polyomavirus family, with an external diameter of 48.4 nm.[11] Its capsid proteins encapsidate a circular double-stranded (ds) DNA genome of 5243 base pairs that is compacted by histone octamers to form a minichromosome-like structure confined within the capsid. SV40 can be used for gene delivery and is known to be capable of infecting nondividing cells, a major limitation of many retroviral vectors used for gene transfer.[12]

The capsid structure of wt SV40, resolved by cryo-TEM[13] and crystallography,[14,15] is an icosahedron with triangulation, *T*, number 7 (*T* = 7).[16] The capsid is built of three different viral encoded proteins (VPs); VP1, VP2, and VP3. Immediately following translation, five VP1 monomers assemble through interdigitating *β*-strands, to form a tightly bound pentamer ($VP1_5$),[14,17] which serves as the basic subunit of the capsid. 72 VP1 pentamers, arranged in a *T* = 7*d* icosahedral symmetry, are forming the outer capsid shell. A molecule of VP2 or VP3 per $VP1_5$ is located in the internal part of the capsid and connects the capsid to the chromatin core. VP1 pentamers occupy two different positions in the capsid shell; 12 pentamers, located at the 12 vertices of the icosahedral structure are forming pentavalent centers, in which each pentamer is surrounded by five other pentamers. The other 60 pentamers occupy hexavalent positions, in which a single pentamer is surrounded by six pentamers.

The crystal structures of the wt SV40 capsid[14,15] and other polyoma viruses revealed that the arrangement in a *T* = 7 icosahedral structure is facilitated by nonequivalent contacts between adjacent VP1 pentamers. The different contacts, *α*, *α*′, *α*″, *β*, *β*′, and *γ* are facilitated by flexible carboxy (C) terminal arms that extend from the jelly roll *β*-barrel VP1 cores. The flexible arms (66 amino acid long) are extended from each VP1 monomer and inserted into a neighboring pentamer. The flexibility of the interactions between identical pentamers enables the icosahedral symmetry of the capsid. The C-arms contain an *α*-helix (amino acids 301−312) segment. *α*- and *β*-contact interactions are predominantly hydrophobic and occur between the helices (three in the *α* contact and two in the *β* contact) of the monomers, taking part in the interaction. *γ* interaction is a tight hydrophobic interaction between adjacent surfaces of two monomers of neighboring pentamers. The different bonding between adjacent pentamers is facilitated through different conformations of a conserved pentapeptide hinge, KNPYP, through proline isomerization.[18]

Calcium ions (Ca^{2+}) and disulfide bonds are involved in the stabilization of the wt SV40 capsid and are playing a role in its

Received: October 10, 2018
Accepted: December 13, 2018
Published: January 2, 2019

DOI: 10.1021/acsomega.8b02753
ACS Omega 2019, 4, 58−64

assembly and disassembly pathways.[12,19−22] Disulfide bonds are formed in VP1 in vivo and lead to folding of the VP1 monomers and to the formation of stable pentamers, the capsid building blocks.[17] Additional disulfide bonds, between cys104, of adjacent pentamers, stabilize the assembled particle.[14] β−β' and α contacts include disulfide bonds, whereas the γ contacts are unlikely to form disulfide bonds. The crystal structure of SV40[14] reveals two potential calcium ions binding sites, anchored between glutamic acid residues. The ions lock the invading C terminal arm of one pentamer to its neighbor and stabilize the α and β inter-pentamer interactions.[23] Mutating the glutamic acid residues to arginines and lysines and mutants of the cysteine residues led to capsids that were unstable to various degrees and affected viral entry and infection.[17,19,20]

Ca^{2+} ions appear to play an important role in the immune evasion by SV40. Following recognition of the GM1 monogangliside[24,25] and additional receptors[26,27] on the cell surface, SV40 enters the cell by endocytosis and is translocated to the endoplasmic reticulum (ER) via the endosomic pathway. Unlike other viruses that undergo conformational changes at the late, acidic endosomes, SV40 is stabilized at acidic pH, perhaps as the glutamic acid and other basic residues at the calcium binding sites become protonated. Therefore, unlike other viruses, SV40 reaches the ER intact, unexposed to the lysosomal and proteosomal degradation, and does not display VP1 antigens at the cell surface. Acid stability, most likely, underlies its immune evasion.

Between 6 and 8 h post infection, the infecting virus undergoes disassembly in the ER, releasing its genetic material that is transported to the nucleus.[27] The release of Ca^{2+} ions, presumably via ER Ca^{2+} homeostasis, is a key factor in SV40 disassembly.[20,28]

VLPs are formed spontaneously in vivo, in the nuclei of insect cells.[12] Capsid formation in vitro requires the addition of a charged polymer scaffold. We therefore term these particles PC-VLPs. The size, shape, and symmetry of the resulting capsid are dictated by the size and rigidity of the polyion scaffold.[29] T = 1 particles form within several milliseconds when VP1 is mixed with 500-mer RNA.[30] When the circular ds-DNA of wt SV40 is used for assembly, a T = 7 capsid is formed. The structure of a T = 7 PC-VLP capsid is similar to that of wt SV40 capsid. PC-VLPs provide a means to study the interactions between the major capsid protein VP1, without the presence of VP2 and VP3.

In this work we have used solution small angle X-ray scattering (SAXS) to determine the structural changes in the capsid of wt SV40 and in T = 7 PC-VLPs encapsidating by SV40 DNA when Ca^{2+} are chelated and disulfide bonds are reduced. SAXS is a bulk method hence statistically reliable and highly sensitive to small changes in the virus dimensions that would be too small to visualize with other methods and under solution conditions. We found that in the presence of both Ca^{2+} chelating and reducing agents, the capsid of wt SV40 and PC-VLPs adopted a swollen conformation. By applying external osmotic pressure to the virus particles, the swollen conformation shrunk back to its original size. Similarly the, SV40-PC-VLPs capsid can be stabilized upon adding Ca^{2+} ions to the assembly solution. Understanding these interactions and their influence on the wt SV40 structure and stability provides insights into the assembly and disassembly of wt SV40, which, in vivo, takes place in the nucleus and ER, respectively, and provides unique means to improve the design of PC-VLPs-based assembly systems.

RESULTS AND DISCUSSION

To better understand the interactions between VP1 pentamers, we studied the effect of calcium and disulfide bonds on the structure of wt SV40 and PC-VLPs. We performed SAXS measurements from wt SV40 and PC-VLPs in saline solution with and without the calcium chelating agent ethylene glycol-bis(2-aminoethylether)-*N*,*N*,*N*′,*N*′-tetraacetic acid (EGTA) and the disulfide bond reducing agent dithiothreitol (DTT).

Figure 1A shows that EGTA by itself did not significantly change the scattering curve. This result suggests that negligible

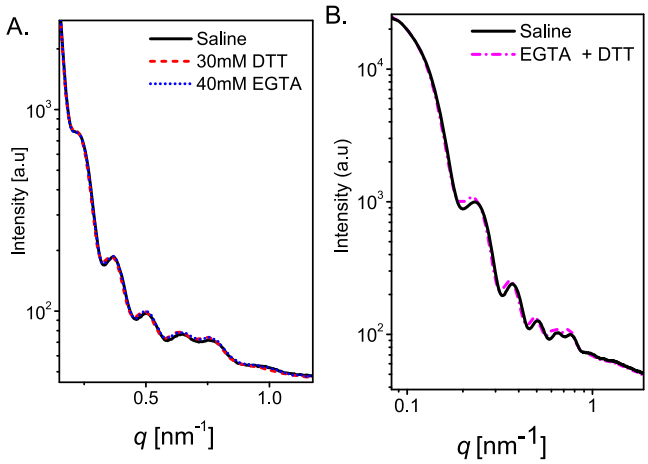

Figure 1. Azimuthally integrated background-subtracted SAXS intensity curves from 3 mg/mL wt SV40. Measurements were performed using our in-house SAXS setup in different solution conditions. The scattering intensity is plotted as a function of q, which is the magnitude of the scattering vector. (A) Saline solution, saline solution with 30 mM DTT, and saline solution with 40 mM EGTA. (B) Saline solution (as in A) and saline solution with both 40 mM EGTA and 30 mM DTT.

structural changes occurred when Ca^{2+} ions were bound to the virus or detached from it. When only DTT was added, the minima of the scattering curve slightly shifted toward lower scattering angles, indicating that the dimensions of the virus slightly increased.

When both EGTA and DTT were added to the saline solution (Figure 1B), the minima clearly shifted to lower scattering angles. The results suggest that the combined effect of Ca^{2+} release and reduction of disulfide bonds led to a significant swelling of wt SV40 and that the two elements depend on one another, in agreement with earlier reports.[19,20,31] This observation suggests that either disulfide bonds or Ca^{2+} bonds were sufficient to keep the capsid close to its original dimensions. When both types of bonds were simultaneously removed, the association between pentamers was sufficiently weaker, hence capsid swelling was achievable.

The results of Figure 1B where then repeated with higher concentrations of EGTA and DTT (Figure 2). To analyze the data in Figure 2, we calibrated lower resolution models of concentric spherical shells against the atomic model of the capsid, taken from protein data bank (PDB) entry 1SVA.[32] We used our home-developed[33] state-of-the-art scattering data analysis software D+ (https://scholars.huji.ac.il/uriraviv/software/d-software), to compute the expected solution scattering

DOI: 10.1021/acsomega.8b02753
ACS Omega 2019, 4, 58−64

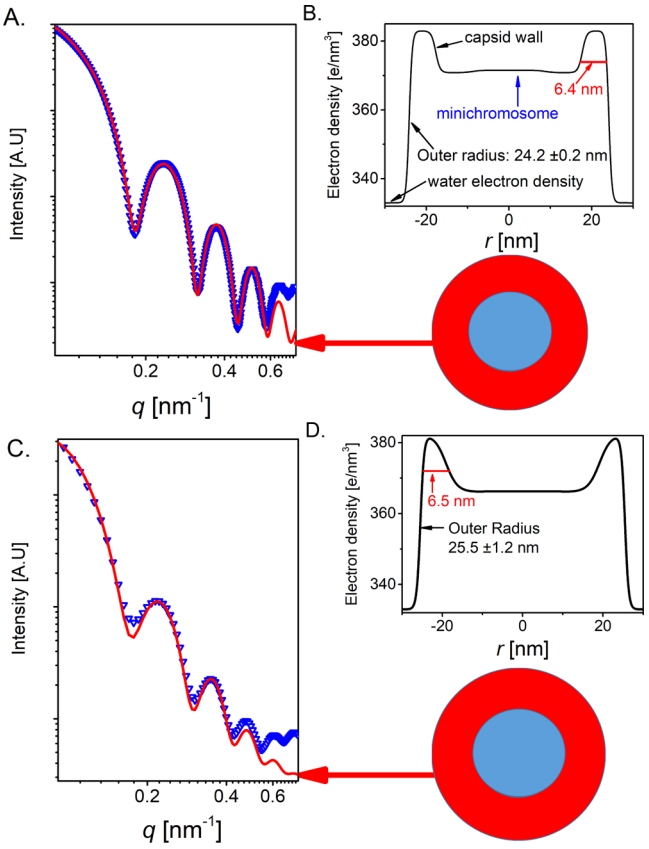

Figure 2. Azimuthally integrated background-subtracted SAXS intensity curves from 1 mg/mL wt SV40 in saline solution (A,B) and in saline solution with both 50 mM EGTA and 50 mM DTT (C,D). The data (blue symbols) were fitted to models (red curves) of concentric spherical shells with radial electron density profiles as shown in (B,D). The cartoons show the electron density profile of the fitted models. The water electron density, capsid wall thicknesses, the outer radii, and the polydispersities of the outer radii are indicated in the figure. The central part of the electron density (shown in blue in the cartoons) corresponds to the electron density of the minichromosome of wt SV40.[35] Models were convolved with an instrument Gaussian resolution function whose standard deviation, σ, was 0.01 nm^{-1}.

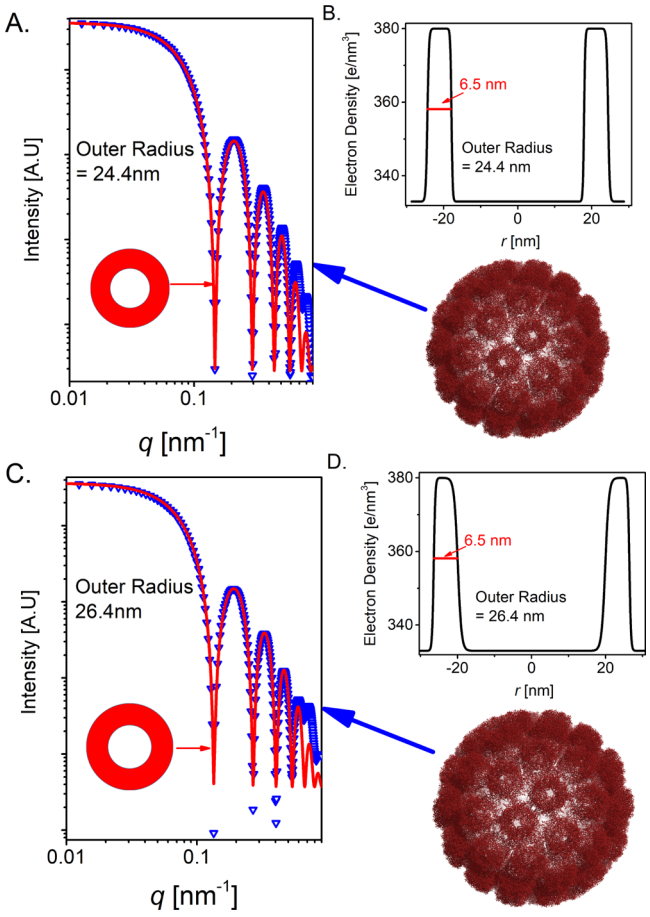

Figure 3. Calibration of geometric capsid models by comparing with the computed scattering curves from atomic models. (A) Atomic model (blue symbols, wine color cartoon), based on PDB entry 1SVA.[32] The geometric centers of pentamers in the PDB was at a radius of 21.3 nm for the vertices and 21.1 nm for the edges. We assumed a hydration layer with an electron density of 364 e/nm^3 and thickness of 0.2 nm. The red curve and red cartoon show the best fitted concentric shell model (B). The electron density profile of the concentric shell models, shown in (A). (C) Atomic model of a swollen capsid in which the geometric centers were multiplied by a factor of 1.1 (blue symbol, wine color cartoon) and the best fitted concentric shell model (red curve and red cartoon). (D) The electron density profile of the concentric shell models, shown in (C). The wall thicknesses and outer radii used in the geometric models (red curves) are indicated in the figure.

curve from the atomic model of the capsid (Figure 3A). We then fitted the result to a geometric model of concentric spherical shells with a radial electron density profile, given by a sum of hyperbolic tangents (Figure 3B), generated as explained in our earlier papers.[34,35] Similar analysis was repeated for a swollen capsid (Figure 3C,D). Figure 4 compares the scattering curves from the two atomic models: the capsid of wt SV40 (Figure 3A) and the swollen SV40 capsid (Figure 3C).

On the basis of the calibration in Figure 3, the data in Figure 2 were fitted to a model of concentric spherical shells with a radial electron density profile, given by a sum of hyperbolic tangents (Figure 2C), generated as explained in our earlier papers.[34,35] The polydispersity of the outer radii was taken into account as explained.[36] The analysis showed that the radius of wt SV40 increased from 24.2 ± 0.2 to 25.5 ± 1.2 nm. The increased polydispersity suggests that the particles could have also slightly changed their shape. The ∼5% increase in the capsid radius led to ∼11% increase in the surface area and ∼17% increase in volume. The spacing between the centers of adjacent pentamers in wt SV40 varies between 8.5 and 10.3 nm.[14,35] The swelling of the particles in the presence of 50 mM DTT and 50 mM EGTA suggests that on average, the distances between pentamers increased by ∼0.5 nm. We attribute this ability to maintain the capsid structure while increasing the distance between subunits, in about 0.5 nm, to the important role of the flexible C arms in increasing the stability of the capsid, by effectively increasing the range of inter-pentamers interaction.

The inner core electron density of 371 e/nm^3 corresponds to the density of the minichromosome. When the particle swelled, the density was supposed to decrease down to 364 e/nm^3, whereas the actual value was 366 e/nm^3. In the future, it will be interesting to perform in situ time-resolved SAXS experiments to elucidate how viral particles are swelling as they are mixed with chelating and/or reducing agents.

DOI: 10.1021/acsomega.8b02753
ACS Omega 2019, 4, 58−64

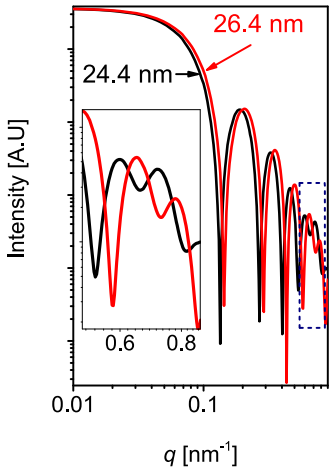

Figure 4. Effect of capsid outer radius. Comparing the scattering curves from the two atomic models in Figure 3. The outer radii of each model are indicated in the figure. The inset shows the higher q-range on an expanded scale.

To isolate the interactions between VP1 pentamers, we studied the effect of Ca^{2+} ions on the structure of PC-VLPs. A solution of soluble VP1 pentamers were prepared by performing dialysis of purified empty VP1 capsids (see Materials and Methods) against 1 mM DTT and 1 mM ethylenediaminetetraacetic acid (EDTA). By mixing VP1 pentamers with wt 5.2 kpb circular ds-DNA, PC-VLPs with a $T = 7$ symmetry were spontaneously assembled.[35] The assembly buffer did not contain Ca^{2+} ions and most likely the VP1 did not have disulfide bonds (see Materials and Methods). The assembly reaction was triggered by binding of the VP1 pentamers to the circular ds-DNA rather than VP1−VP1 interaction. This binding was facilitated by the net positive charge of the VP1 pentamer side that is facing the capsid lumen[14] and the net negative change on the DNA. Both the DNA and VP1 pentamers were neutralized by monovalent counterions. The association between the DNA and VP1 pentamers was driven by the release of their counterions into the solution because the DNA and VP1 could neutralize each other. When the counterions were released, they gained solution entropy, which lowered the total free energy.

Figure 5 shows that without Ca^{2+} ions, the PC-VLP had an outer radius of 26.6 ± 1.0 nm, which is about 2 nm larger than wt SV40. When 4 mM $CaCl_2$ was added to the solution, the radius of the PC-VLP decreased to 25.3 nm, which is much closer to that of wt SV40. The density profiles in Figure 5B,D, show thicker walls, suggesting that the DNA was still forced against the wall, thus exerting internal pressure on the capsid wall, which may explain the slightly larger radius, compared with wt SV40. The compaction of the PC-VLP by the Ca^{2+} ions was therefore, most likely, owing to strengthening of capsid protein−protein interaction, rather than a decrease in the PC-VLP internal pressure. In both particles, the inner cavity had electron density close to bulk water, suggesting the particles were empty.

To study the effect of moderate osmotic pressure, we put 26 μL of 3 mg/mL wt SV40 solution in a quartz capillary. 4 μL of 40 wt % 20 kD poly(ethylene glycol) (PEG) solution in water were then added to the virus solution. The added PEG solution led to precipitation of the virus particles into a condensed phase at the bottom of the capillary. The precipitant was formed owing to the moderate osmotic

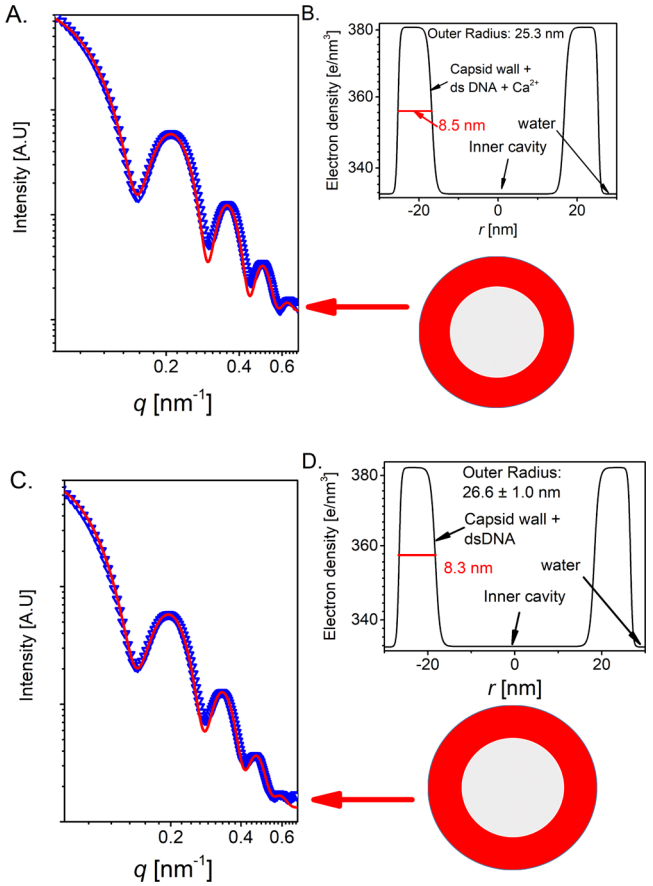

Figure 5. Azimuthally integrated background-subtracted SAXS intensity curves from PC-VLPs (blue symbols). 8.5 μM VP1 were mixed with the wt circular 5.2 kbp ds-DNA in a molar ratio of 144:1 in saline solutions containing 4 mM $CaCl_2$ (A,B) and in saline solution (C,D). The data were fitted to models of concentric spherical shells (red curves and cartoons) with radial electron density profiles as shown in (B,D). The wall thicknesses, outer radii, and outer radius polydispersities are indicated in the figure. Models were convolved with an instrument Gaussian resolution function whose standard deviation, σ, was 0.015 nm^{-1}.

pressure (of about 25 kPa), which was applied by the PEG solution. The PEG was excluded from the particles and led to depletion attraction between them.[37,38] Figure 6 shows that the minima in the scattering curve shifted to higher scattering angles. This result suggests (see Figure 4) that the osmotic pressure also decreased the capsid dimensions, owing to transport of water molecules from the inner volume of the virus toward the PEG solution, at which their chemical potential was lower. Water removal forced the capsid proteins to get closer to one another, and the virus adopted a tighter conformation. Larger structural changes were not observed under the rather moderate osmotic stress used in this study.

Addition of EGTA and DTT lead to swelling of the capsid (Figure 1). We attribute the swelling to weakening of the interaction between pentamers either by reduction of the disulfide bonds or by the release of Ca^{2+} ions. The swollen structure, enabled to explore a wider range of conformational space. Figure 6 shows that applying osmotic stress to wt SV40 in the swollen conformation, recouped the structure of native wt SV40 under similar osmotic stress. Upon addition of PEG, a precipitate formed, suggesting that the density of virus particles increased, consistent with the observed structure-factor peaks

DOI: 10.1021/acsomega.8b02753
ACS Omega 2019, 4, 58−64

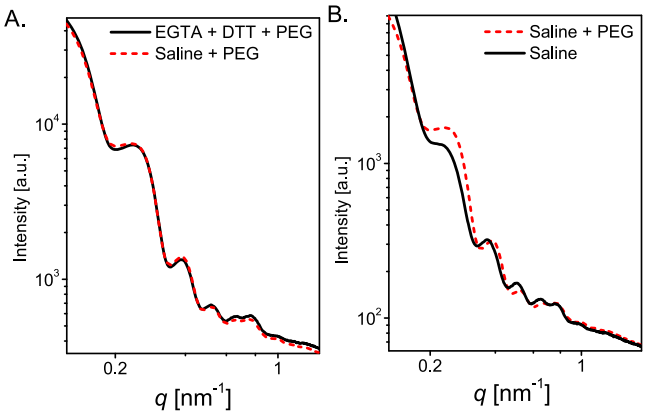

Figure 6. Azimuthally integrated background-subtracted SAXS intensity curves from 3 mg/mL wt SV40 with 5 wt % 20 kD PEG. Measurements were performed using our in-house SAXS setup in saline solution, and in saline solution with both 40 mM EGTA and 30 mM DTT (A). In (B), we compare the measured scattering intensities in saline solution with and without added PEG.

at the lower q-range. The behavior at the higher q-range is consistent with a small decrease of the outer capsid radius (see Figure 4).

We note that the concentration of chelating and reducing agents in vivo are at least an order of magnitude lower than used here. When we dialyzed wt SV40 particles against solutions with 2 mM DTT and 2 mM EGTA, similar results were obtained. At 5 mM concentrations, it has been recently shown that DTT makes DNA-containing VLPs less resistant to mechanical stress and prone to damage, whereas EDTA induces a marked softening of the particles.[39]

CONCLUSIONS

In this paper, we showed that both calcium ions and disulfide bonds stabilized the structure of wt SV40 and PC-VLPs. When only calcium ions were removed, the structure of wt SV40 remained nearly unchanged. Reducing disulfide bonds led to a slight swelling of wt SV40. When both calcium ions were chelated and disulfide bonds were reduced, the volume of wt SV40 increased by about 17% and the spacing between pentamers increased by about 5% (or 0.5 nm). The swelling of the virus could be reversed by applying osmotic pressure using PEG solution. PC-VLPs formed by mixing VP1 and the wt circular ds-DNA showed similar behavior. The volume changes were attributed to the interactions between the capsid proteins rather than to the internal pressure in the particles.

MATERIALS AND METHODS

Samples Preparation for SAXS Measurements. wt SV40 was purified as explained in our earlier paper.[11] The control wt SV40 sample was measured in saline (0.9 wt % NaCl). The other samples were either mixed with EGTA and DTT and/or 20 kD PEG solutions. The samples were then equilibrated at ambient room temperature for about an hour, before they were transferred to the measurement cell.

Virus-like particles were formed by a disassembly-reassembly protocol in a similar way to our earlier study.[30] Purified empty VP1 capsids were dialyzed twice against two disassembly buffers. The first buffer contained 50 mM NaCl, 20 mM Tris at pH 8.9, 5 mM EDTA, and 2 mM DTT. In the second dialysis, the disassembly buffer contained 50 mM NaCl, 20 mM Tris at pH 8.9, 2 mM EDTA and 2 mM DTT. Hence, the resulting VP1 pentamers did not contain Ca^{2+} or disulfide bonds.

VP1 pentamers solution at concentration of 17 μM was mixed at a volume ratio of 1:1 with a solution containing the wt SV40 circular ds-DNA at a concentration of 0.12 μM with and without 4 mM $CaCl_2$. The final solution of the assembled particles contained 150 mM NaCl, 1 mM, EDTA, 1 mM DTT, and 0 or 4 mM $CaCl_2$.

SAXS Measurement Setup and Data Reduction. SAXS measurements of the wt SV40 presented in Figures 1 and 6 were performed in our in-house setup, described in our earlier paper.[40] A background measurement was taken before the sample using the same capillary. SAXS results presented in Figure 2 were performed using the flow cell setup in the SWING beamline at Soleil Synchrotron (GIF-sur-YVETTE)[41] and in the P12 beamline of the EMBL located at the PETRA III storage ring (DESY, Hamburg).[42] The PC-VLPs were measured in the flow-cell setup at ID02 beamline in ESRF (Grenoble).[43] All measurements were taken at room temperature and buffer background measurements were taken before and after each virus sample. Data reduction was performed as explained in ref 11. The averaged background signals were then subtracted from the averaged samples signals.

Extracting the Radius of Virus Particles. The scattering intensity from noninteracting N virus particles is given by, $I_{N\ \mathrm{virus\ particles}}(q) = NI_{\mathrm{virus}}(q)$, where $I_{\mathrm{virus}}(q)$ is the scattering intensity of a single soluble virus given by

$$I_{\mathrm{virus}}(q) = \langle |\mathrm{FF}(\vec{q})|^2 \rangle = \left\langle \left| - r_0 \int_V \Delta\rho(\vec{r}) \exp\{-i\vec{q}\cdot\vec{r}\}\, \mathrm{d}\vec{r} \right|^2 \right\rangle \quad (1)$$

where the form factor, FF, is the Fourier transform of the electron density contrast of the virus with respect to the solvent, $\Delta\rho(\vec{r})$. $\vec{q}$ is the elastic momentum transfer vector. The brackets $\langle\ \rangle$ represent average over time and virus orientations in the solution. At low resolution, the virus particle can be approximately considered as spherical. This assumption holds up to a resolution at which the inter-pentamer correlations contribute significantly to the scattering intensity as was previously shown.[11,35] In order to determine the change in the outer radius of the particles at different chemical environments, the lower q range of the resulting 1D data, was analyzed using the X+ (https://scholars.huji.ac.il/uriraviv/software/x) software developed in our lab[34,36,44] and our recent[33,45] state-of-the-art analysis software D+. The analysis with X+ was done with a model of concentric spheres with a radial electron density profile that was constructed from a sum of hyperbolic tangents as explained in our earlier papers.[34,35] The model was then fitted to the scattering data by adjusting the thickness and electron density of each layer, and three layers or less were needed to obtained the best fit.

Using our home developed software D+, we computed the scattering from the atomic model of the capsid, based on protein data bank entry 1SVA.[32] By comparing the resulting scattering curve of the atomic model with that of a concentric sphere model with a radial electron density profile (Figure 3), we calibrated the electron density and thickness of the capsid wall. The calculation was performed with the outer wall radius of the capsid crystal structure, 24.4 nm (Figure 3A,B), and a swollen capsid with an outer wall radius of 26.4 nm (Figure

DOI: 10.1021/acsomega.8b02753
ACS Omega 2019, 4, 58−64

3C,D). The calibration reduced the number of free parameters in the concentric shell model.

AUTHOR INFORMATION

Corresponding Author

*E-mail: uri.raviv@mail.huji.ac.il. Phone: +972-2-6586030. Fax: +972-2-566-0425.

ORCID

Uri Raviv: 0000-0001-5992-9437

Notes

The authors declare no competing financial interest.

ACKNOWLEDGMENTS

We thank Daniel Harries for helpful discussion. We thank Desy synchrotron at Hamburg, beamline P12 (D. Svergun and his team), Soleil synchrotron, Swing beamline (J. Perez and his team), and the ESRF synchrotron, ID02 beamline (T. Narayanan and his team) for provision of synchrotron radiation facilities and for assistance in using the beamlines. This project was supported by the Israel Science Foundation (656/17), the United States-Israel Binational Science Foundation (2016311), and the NIH (Award number 1R01AI118933). R.A. acknowledges support from the Kaye-Einstein fellowship foundation.

ABBREVIATIONS

SAXS, small-angle X-ray scattering; wt SV40, wild-type simian virus 40; VLP, virus-like particles; PC-VLP, polymer-containing virus-like particles; ds-DNA, double-stranded DNA; VP, virus protein; ER, endoplasmic reticulum; EGTA, ethylene glycol-bis(2-aminoethylether)-*N*,*N*,*N*′,*N*′-tetraacetic acid; DTT, dithiothreitol; PEG, poly(ethyleneglycol)

REFERENCES

(1) Casselyn, M.; Perez, J.; Tardieu, A.; Vachette, P.; Witz, J.; Delacroix, H. Spherical plant viruses: interactions in solution, phase diagrams and crystallization of brome mosaic virus. *Acta Crystallogr., Sect. D: Biol. Crystallogr.* **2001**, *57*, 1799−1812.

(2) Auyeung, E.; Li, T. I. N. G.; Senesi, A. J.; Schmucker, A. L.; Pals, B. C.; de la Cruz, M. O.; Mirkin, C. A. DNA-mediated nanoparticle crystallization into Wulff polyhedra. *Nature* **2013**, *505*, 73−77.

(3) Schwarz, B.; Uchida, M.; Douglas, T. Biomedical and Catalytic Opportunities of Virus-Like Particles in Nanotechnology. *Adv. Virus Res.* **2017**, *97*, 1−60.

(4) Pokorski, J. K.; Steinmetz, N. F. The art of engineering viral nanoparticles. *Mol. Pharmacol.* **2011**, *8*, 29.

(5) Loo, L.; Guenther, R. H.; Basnayake, V. R.; Lommel, S. A.; Franzen, S. Controlled encapsidation of gold nanoparticles by a viral protein shell. *J. Am. Chem. Soc.* **2006**, *128*, 4502−4503.

(6) Chen, C.; Daniel, M.-C.; Quinkert, Z. T.; De, M.; Stein, B.; Bowman, V. D.; Chipman, P. R.; Rotello, V. M.; Kao, C. C.; Dragnea, B. Nanoparticle-templated assembly of viral protein cages. *Nano Lett.* **2006**, *6*, 611−615.

(7) Douglas, T. Viruses: making friends with old foes. *Science* **2006**, *312*, 873−875.

(8) Uchida, M.; Klem, M. T.; Allen, M.; Suci, P.; Flenniken, M.; Gillitzer, E.; Varpness, Z.; Liepold, L. O.; Young, M.; Douglas, T. Biological containers: protein cages as multifunctional nanoplatforms. *Adv. Mater.* **2007**, *19*, 1025−1042.

(9) Jordan, P. C.; Patterson, D. P.; Saboda, K. N.; Edwards, E. J.; Miettinen, H. M.; Basu, G.; Thielges, M. C.; Douglas, T. Self-assembling biomolecular catalysts for hydrogen production. *Nat. Chem.* **2015**, *8*, 179.

(10) Roosen-Runge, F.; Heck, B. S.; Zhang, F.; Kohlbacher, O.; Schreiber, F. Interplay of pH and binding of multivalent metal ions: charge inversion and reentrant condensation in protein solutions. *J. Phys. Chem. B* **2013**, *117*, 5777−5787.

(11) Asor, R.; Ben-nun-Shaul, O.; Oppenheim, A.; Raviv, U. Crystallization, Reentrant Melting, and Resolubilization of Virus Nanoparticles. *ACS Nano* **2017**, *11*, 9814−9824.

(12) Sandalon, Z.; Oppenheim, A. Self-Assembly and Protein-Protein Interactions between the SV40 Capsid Proteins Produced in Insect Cells. *Virology* **1997**, *237*, 414−421.

(13) Baker, T. S.; Drak, J.; Bina, M. Reconstruction of the three-dimensional structure of simian virus 40 and visualization of the chromatin core. *Proc. Natl. Acad. Sci. U.S.A.* **1988**, *85*, 422−426.

(14) Stehle, T.; Gamblin, S. J.; Yan, Y.; Harrison, S. C. The structure of simian virus 40 refined at 3.1 å resolution. *Structure* **1996**, *4*, 165−182.

(15) Liddington, R. C.; Yan, Y.; Moulai, J.; Sahli, R.; Benjamin, T. L.; Harrison, S. C. Structure of simian virus 40 at 3.8-Å resolution. *Nature* **1991**, *354*, 278.

(16) Caspar, D. L.; Klug, A. Physical principles in the construction of regular viruses. *Cold Spring Harbor Symposia On Quantitative Biology*, 1962; pp 1−24.

(17) Li, P. P.; Nakanishi, A.; Clark, S. W.; Kasamatsu, H. Formation of transitory intrachain and interchain disulfide bonds accompanies the folding and oligomerization of simian virus 40 Vp1 in the cytoplasm. *Proc. Natl. Acad. Sci. U.S.A.* **2002**, *99*, 1353−1358.

(18) Ben-nun-Shaul, O.; Bronfeld, H.; Reshef, D.; Schueler-Furman, O.; Oppenheim, A. The SV40 capsid is stabilized by a conserved pentapeptide hinge of the major capsid protein VP1. *J. Mol. Biol.* **2009**, *386*, 1382−1391.

(19) Li, P. P.; Naknanishi, A.; Tran, M. A.; Ishizu, K.-I.; Kawano, M.; Phillips, M.; Handa, H.; Liddington, R. C.; Kasamatsu, H. Importance of Vp1 calcium-binding residues in assembly, cell entry, and nuclear entry of simian virus 40. *J. Virol.* **2003**, *77*, 7527−7538.

(20) Kawano, M.-a.; Xing, L.; Tsukamoto, H.; Inoue, T.; Handa, H.; Cheng, R. H. Calcium-bridge triggers capsid disassembly in the cell entry process of simian virus 40. *J. Biol. Chem.* **2009**, *284*, 34703.

(21) Christiansen, G.; Landers, T.; Griffith, J.; Berg, P. Characterization of components released by alkali disruption of simian virus 40. *J. Virol.* **1977**, *21*, 1079−84.

(22) Brady, J. N.; Lavialle, C.; Salzman, N. P. Efficient transcription of a compact nucleoprotein complex isolated from purified simian virus 40 virions. *J. Virol.* **1980**, *35*, 371−381.

(23) Brady, J. N.; Winston, V. D.; Consigli, R. A. Dissociation of polyoma virus by the chelation of calcium ions found associated with purified virions. *J. Virol.* **1977**, *23*, 717−724.

(24) Smith, A. E.; Lilie, H.; Helenius, A. Ganglioside-dependent cell attachment and endocytosis of murine polyomavirus-like particles. *FEBS Lett.* **2003**, *555*, 199−203.

(25) Tsai, B.; Gilbert, J. M.; Stehle, T.; Lencer, W.; Benjamin, T. L.; Rapoport, T. A. Gangliosides are receptors for murine polyoma virus and SV40. *EMBO J.* **2003**, *22*, 4346−4355.

(26) Szklarczyk, O. M.; González-Segredo, N.; Kukura, P.; Oppenheim, A.; Choquet, D.; Sandoghdar, V.; Helenius, A.; Sbalzarini, I. F.; Ewers, H. Receptor concentration and diffusivity control multivalent binding of Sv40 to membrane bilayers. *PLoS Comput. Biol.* **2013**, *9*, No. e1003310.

(27) Kobiler, O.; Drayman, N.; Butin-Israeli, V.; Oppenheim, A. Virus strategies for passing the nuclear envelope barrier. *Nucleus* **2014**, *3*, 526−539.

(28) Schelhaas, M.; Malmström, J.; Pelkmans, L.; Haugstetter, J.; Ellgaard, L.; Grünewald, K.; Helenius, A. Simian Virus 40 depends on ER protein folding and quality control factors for entry into host cells. *Cell* **2007**, *131*, 516−529.

(29) Kler, S.; Wang, J. C.-Y.; Dhason, M.; Oppenheim, A.; Zlotnick, A. Scaffold properties are a key determinant of the size and shape of self-assembled virus-derived particles. *ACS Chem. Biol.* **2013**, *8*, 2753−2761.

(30) Kler, S.; Asor, R.; Li, C.; Ginsburg, A.; Harries, D.; Oppenheim, A.; Zlotnick, A.; Raviv, U. RNA encapsidation by SV40-derived

DOI: 10.1021/acsomega.8b02753
ACS Omega 2019, 4, 58−64

nanoparticles follows a rapid two-state mechanism. *J. Am. Chem. Soc.* **2012**, *134*, 8823−8830.
(31) Mukherjee, S.; Kler, S.; Oppenheim, A.; Zlotnick, A. Uncatalyzed assembly of spherical particles from SV40 VP1 pentamers and linear dsDNA incorporates both low and high cooperativity elements. *Virology* **2010**, *397*, 199−204.
(32) Stehle, T.; Yan, Y.; Benjamin, T. L.; Harrison, S. C. Structure of murine polyomavirus complexed with an oligosaccharide receptor fragment. *Nature* **1994**, *369*, 160.
(33) Ginsburg, A.; Ben-Nun, T.; Asor, R.; Shemesh, A.; Fink, L.; Tekoah, R.; Levartovsky, Y.; Khaykelson, D.; Raviv, U. D+: Software for High-Resolution Hierarchical Modeling of Solution X-Ray Scattering from Complex Structures, **2018** DOI: 10.26434/chemrxiv.7012622,
(34) Ben-Nun, T.; Asor, R.; Ginsburg, A.; Raviv, U. Solution X-ray Scattering Form-Factors with Arbitrary Electron Density Profiles and Polydispersity Distributions. *Isr. J. Chem.* **2015**, *56*, 622.
(35) Saper, G.; Kler, S.; Asor, R.; Oppenheim, A.; Raviv, U.; Harries, D. Effect of capsid confinement on the chromatin organization of the SV40 minichromosome. *Nucleic Acids Res.* **2012**, *41*, 1569−1580.
(36) Ben-Nun, T.; Ginsburg, A.; Székely, P.; Raviv, U. X+: a comprehensive computationally accelerated structure analysis tool for solution X-ray scattering from supramolecular self-assemblies. *J. Appl. Crystallogr.* **2010**, *43*, 1522−1531.
(37) Asakura, S.; Oosawa, F. Interaction between particles suspended in solutions of macromolecules. *J. Polym. Sci.* **1958**, *33*, 183−192.
(38) Sapir, L.; Harries, D. Is the depletion force entropic? Molecular crowding beyond steric interactions. *Curr. Opin. Colloid Interface Sci.* **2015**, *20*, 3−10.
(39) van Rosmalen, M. G. M.; Li, C.; Zlotnick, A.; Wuite, G. J. L.; Roos, W. H. Effect of dsDNA on the Assembly Pathway and Mechanical Strength of SV40 VP1 Virus-like Particles. *Biophys. J.* **2018**, *115*, 1656−1665.
(40) Nadler, M.; Steiner, A.; Dvir, T.; Szekely, O.; Szekely, P.; Ginsburg, A.; Asor, R.; Resh, R.; Tamburu, C.; Peres, M.; et al. Following the structural changes during zinc-induced crystallization of charged membranes using time-resolved solution X-ray scattering. *Soft Matter* **2011**, *7*, 1512−1523.
(41) David, G.; Pérez, J. Combined sampler robot and high-performance liquid chromatography: a fully automated system for biological small-angle X-ray scattering experiments at the Synchrotron SOLEIL SWING beamline. *J. Appl. Crystallogr.* **2009**, *42*, 892−900.
(42) Blanchet, C. E.; Spilotros, A.; Schwemmer, F.; Graewert, M. A.; Kikhney, A.; Jeffries, C. M.; Franke, D.; Mark, D.; Zengerle, R.; Cipriani, F.; et al. Versatile sample environments and automation for biological solution X-ray scattering experiments at the P12 beamline (PETRA III, DESY). *J. Appl. Crystallogr.* **2015**, *48*, 431−443.
(43) Van Vaerenbergh, P.; Léonardon, J.; Sztucki, M.; Boesecke, P.; Gorini, J.; Claustre, L.; Sever, F.; Morse, J.; Narayanan, T. An upgrade beamline for combined wide, small and ultra small-angle X-ray scattering at the ESRF. *AIP Conf. Proc.* **2016**, *1741*, 030034.
(44) Székely, P.; Ginsburg, A.; Ben-Nun, T.; Raviv, U. Solution X-ray scattering form factors of supramolecular self-assembled structures. *Langmuir* **2010**, *26*, 13110−13129.
(45) Ginsburg, A.; Ben-Nun, T.; Asor, R.; Shemesh, A.; Ringel, I.; Raviv, U. Reciprocal grids: a hierarchical algorithm for computing solution x-ray scattering curves from supramolecular complexes at high resolution. *J. Chem. Inf. Model.* **2016**, *56*, 1518−1527.

DOI: 10.1021/acsomega.8b02753
ACS Omega 2019, 4, 58−64